Fault transmissibility multipliers for flow simulation models

T. Manzocchi[1], J. J. Walsh[1], P. Nell[1] and G. Yielding[2]
[1]*Fault Analysis Group, Department of Earth Sciences, University of Liverpool, Liverpool L69 3BX, UK*
[2]*Badley Earth Sciences Ltd, North Beck Lane, Hundleby, Spilsby, Lincolnshire PE23 5NB, UK*

ABSTRACT: Fault zone properties are incorporated in production flow simulators using transmissibility multipliers. These are a function of properties of the fault zone and of the grid-blocks to which they are assigned. Consideration of the geological factors influencing the content of fault zones allows construction of high resolution, geologically driven, fault transmissibility models. Median values of fault permeability and thickness are predicted empirically from petrophysical and geometrical details of the reservoir model. A simple analytical up-scaling scheme is used to incorporate the influence of likely small-scale fault zone heterogeneity. Fine-scale numerical modelling indicates that variability in fault zone permeability and thickness should not be considered separately, and that the most diagnostic measure of flow through a heterogeneous fault is the arithmetic average of the permeability to thickness ratio. The flow segregation through heterogeneous faults predicted analytically is closely, but not precisely, matched by numerical results. Identical faults have different equivalent permeabilities which depend, in part, on characteristics of the permeability field in which they are contained.

KEYWORDS: *fault (geology), permeability, scale up, flow model, reservoir model*

INTRODUCTION

Faults influence flow in a reservoir simulation model in two ways. First, they alter the connectivity of sedimentological flow units. Displacements across faults can cause partial or total juxtaposition of different flow units, possibly connecting stratigraphically disconnected high permeability units, as well as juxtaposing high against low permeability units. For faults incorporated discretely in flow simulation models, these effects are captured as a function of the relative depths of the corners of the grid-blocks separated by a fault. Faults generally increase the overall vertical connectivity of a reservoir and decrease the overall horizontal connectivity, but the precise influence of fault displacements on reservoir connectivity is complex, as seismic data cannot resolve details of fault structure: what appears to be a single fault on seismic often comprises multiple fault strands which can have a significantly different effect on flow unit connectivity than a single strand (e.g. Childs *et al.* 1997; Knipe 1997). This paper does not address these relatively large-scale connectivity effects which can be analysed with Allan diagrams (Allan 1989), with sequence/throw juxtaposition diagrams (e.g. Bentley & Barry 1991; Knipe 1997) or with aggregate connectivity plots (e.g. Childs *et al.* 1997). Instead we focus on the second influence of faults on flow, arising from the petrophysical properties of the fault-rock.

The effects of the fault-rock properties are conventionally incorporated in a flow simulator using transmissibility multipliers. Lia *et al.* (1997) found fault transmissibility to present by far the greatest uncertainty in reserves estimates for the Veslefrikk Field (Norwegian North Sea), and this uncertainty is due, in part, to the lack of a method for calculating transmissibilities. In this paper we outline and discuss a new, geologically driven method for determining fault transmissibility multipliers as a function of known properties of the reservoir model. The proposed method aims to predict fault zone properties and to capture the influence of unresolved fault zone structure in sandstone/shale sequences using a simple algorithm. Inevitably the method requires assumptions and approximations, and few quantitative data exist to condition the resultant model. The model, therefore, needs calibration against dynamic reservoir data but considerable uncertainty will always be associated with the fault transmissibility determinations due to the natural unpredictability of fault zone structure and content.

Fault permeability and thickness are physically observable properties of fault zones, whilst transmissibility multipliers are numerical devices used *in lieu* of these properties. As the permeability and thickness of sub-surface faults can be estimated, albeit imprecisely, it seems sensible that these estimates be used to determine the transmissibility multipliers for faults in reservoirs for which no dynamic data are available. The use of dynamic data in conditioning faulted simulation models is beyond the scope of this contribution, which aims only to present a method for determining transmissibility multipliers based on a static geological prediction. Dynamic information, where available, provides the only firm indication of the behaviour of any particular fault in a reservoir and must therefore be the prime data conditioning the overall transmissibility assigned to the fault. Nonetheless, an appreciation of the dependencies contained within fault transmissibility multipliers is necessary if the dynamic information is used to construct models which not only match the production and pressure history, but are also geologically palatable.

FAULT ZONE MODEL

Faults in reservoirs are sampled either at low resolution by seismic or at a high resolution by wells. Seismic interpretation provides information about the locations and displacements of

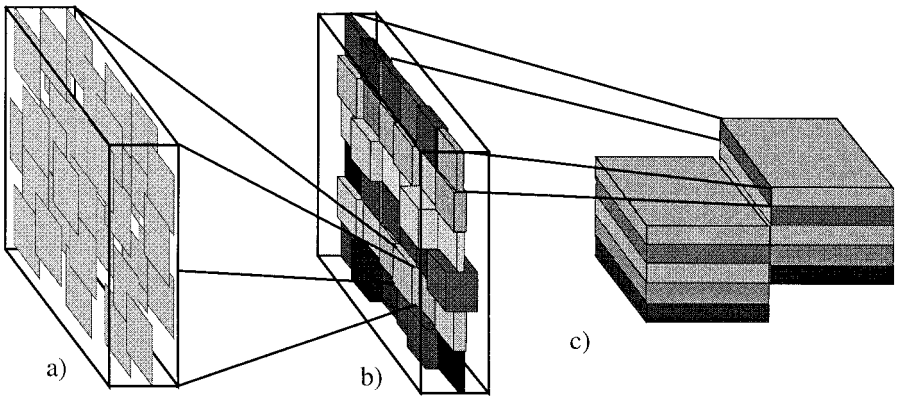

Fig. 1. Conceptual up-scaling hierarchy. (**a**) At the sub-metre scale, the fault-rock permeability is a function of its shale content. (**b**) At the sub-grid-block scale, the fault zones are considered heterogeneous in permeability and thickness. (**c**) At the grid-block scale each grid-block connection is assigned a uniform transmissibility.

large faults, but cannot resolve the small-scale structure within the fault zone. Wells sample faults at a particular point in a reservoir, and cored faults provide direct samples from which fault zone properties can be measured. Fault zones are complex heterogeneous and anisotropic volumes of varying composition and thickness, and a well samples only a single line through a zone. Predicting flow through a fault requires a model of fault zone structure at a resolution which cannot be obtained from either data source. The conceptual model we consider for the determination of fault transmissibility multipliers is shown in Fig. 1.

At the smallest scale, the fault is conceptualized as a volume of a particular thickness and shale content (Fig. 1a), and the proportion of shale in the volume is assumed to be the main control on the fault permeability. The shale content of the fault zone is calculated as a function of the faulted sequence using the Shale Gouge Ratio method (described in the following section). The displacement of a fault is assumed to be the main control on fault zone thickness, and a secondary control on fault zone permeability. At an intermediate scale (Fig. 1b), thickness and permeability are assumed to be log-normally distributed with 75% of the values covering two orders of magnitude around the median value. The correlation-lengths of this heterogeneity are assumed to be substantially smaller than the simulation grid-block size. At the simulation grid-block scale (Fig. 1c), the transmissibility multiplier assigned to each grid-block fault-face is an appropriately up-scaled representation of this heterogeneous fault zone. We do not attempt to capture effects of cement seals, which are the least predictable fault seal type.

Fault zone permeability anisotropy or the influence of fault zones on two-phase flow have not been considered, as neither can be incorporated in a production flow simulation model which uses only transmissibility multipliers to represent fault zone properties. Fault zones can have permeability anisotropies of about 2–3 orders of magnitude (e.g. Evans *et al.* 1997) which, dependent on the pressure gradient, can result in preferential flow parallel to the fault, but the multiplier acts only on flow perpendicular to the fault. The multiplier modifies the absolute grid-block permeability, yet the characteristics of fault gouge will also influence the capillary pressure and relative permeability curves of the up-scaled volume. Neglecting two-phase flow properties of fault zones will suppress capillary trapping behind faults (e.g. Manzocchi *et al.* 1998), as using a transmissibility multiplier to represent the fault increases the overall viscous/capillary ratio of the system. These flow aspects would require that the fault be incorporated using discrete grid-blocks, which would greatly increase the complexity of faulted reservoir models and is therefore not standard practice.

The remainder of this section describes in more detail the background and assumptions of the methods used, which are based on empirical geological observations of static reservoir and outcrop analogue data. The nomenclature used throughout is given in Table 1.

Fault zone permeability

Over recent years a methodology has emerged for the analysis of the seal capacity of faults in sandstone/shale sequences (e.g. Bouvier *et al.* 1989; Gibson 1994; Fristad *et al.* 1997; Yielding *et al.* 1997). These methods do not try to resolve precise details of the structure of fault zones, but instead use proxy-properties to make inferences about the behaviour of a fault, through empirical correlations with other faults of known behaviour in the same hydrocarbon province. The most versatile proxy-property is the Shale Gouge Ratio (SGR). SGR is the proportion of phyllosilicate which has been displaced past any particular point on a fault (e.g. Yielding *et al.* 1997). The minimum SGR on the fault surface is assumed to have the lowest capillary entry pressure, and databases comparing pressure difference supported across faults, with SGR mapped onto the fault surface, are used to assess the integrity of unproven fault traps. These studies suggest that an SGR greater than about 15–20% results in a membrane seal (Watts 1987) capable of separating fluids of different phases. This cut-off is supported by outcrop characterization which shows that faults with SGRs in excess of this value have at least one shale layer within the fault zone which is continuous over the outcrop (e.g. Lindsay *et al.* 1993; Foxford *et al.* 1998). Cut-off values

Table 1. *Nomenclature*

Symbol	Meaning
A	Grid-block area perpendicular to L (m^2)
D	Fault displacement (m)
k	Permeability (mD)
L	Grid-block length (m)
P	Pressure (bars)
q	Flow rate parallel to L ($m^3\,s^{-1}$)
SGR	Fractional shale gouge ratio
t	Thickness (m)
T	Transmissibility (or permeability) multiplier
Trans	Transmissibility (mDm^{-1})
V_{shale}	Fractional phyllosilicate content
μ	Viscosity (cp)
Subscripts	
a	Arithmetic average
f	Fault
h	Harmonic average
i, j, k	Particular grid-blocks
m	Grid-block

also appear to be transferable between different hydrocarbon provinces (Yielding *et al.* 1997).

We make the assumption suggested by Yielding *et al.* (1997), that SGR is equivalent to the shale content (Vshale) of the fault gouge. This assumption is useful as, although it is possible to calculate the SGR for a sub-surface fault zone, the precise shale content of the zone cannot be predicted directly. Available plug permeability data, on the other hand, are recorded as a function of the volumetric shale fraction of the core plugs which are taken as representative of the fault zone.

Figure 2 shows plug and probe permeability data for various reservoir and out-crop fault-rock samples (Antonellini & Aydin 1994; Knai 1996; Gibson 1998; Ottesen Ellevset *et al.* in press). The data show a general decrease in fault zone permeability with increasing shale content, and large variations in permeability at a particular shale content. At very low shale content there is an apparently bimodal distribution governed by fault displacement, demonstrated by the data from Antonellini & Aydin (1994). These data are probe permeameter measurements from samples of the Moab (Vshale=0) and Slickrock (average Vshale=0.09) members of the Entrada Sandstone formation. The clean Moab Sandstone shows a clear distinction between the permeability of deformation bands (displacements in the range 1 mm to a few centimetres and average fault-rock permeabilities of about 10 mD) and slip surfaces (displacements greater than about 1 m, and average permeabilities of less than 0.01 mD). In the more shaley Slickrock member, the permeabilities of deformation bands and slip surfaces are similar to each other, with average values around 0.8 mD. A decrease in the influence of displacement on fault permeability with increasing shale content is caused by these differences in deformation style. In pure sandstone, cataclastic intensity increases with displacement (e.g. Crawford 1998), ultimately resulting in highly polished, intensely cataclastic slip surfaces with exceptionally low permeabilities. Deformation bands in more shaly sandstone are less cataclastic, as displacement is accommodated by small-scale smearing of the phyllosilicates (e.g. Antonellini *et al.* 1994), and the main control on fault permeability is the shale content of the fault.

The curves on Fig. 2 show an empirical prediction of fault zone permeability as a function of shale content and displacement. The curves are given by the equation:

$$\log k_f = -4\mathrm{SGR} - \frac{1}{4}\log(D)(1-\mathrm{SGR})^5 \qquad (1)$$

where k_f is fault permeability (in mD) and D is fault displacement (in metres). We assume that the value of k_f obtained is the median value of a log-normal permeability distribution covering about two orders of magnitude. Therefore, for D=20 m, SGR=0.2, predicted k_f lies in the range 0.012 mD$<k_f<$ 1.2 mD, and the median value is 0.12 mD. The influence of displacement on fault zone permeability in this relationship is not as great at very low shale content as the data on Fig. 2 suggest. Therefore Equation 1 does not provide a reliable estimate of permeability as SGR$\rightarrow$0.

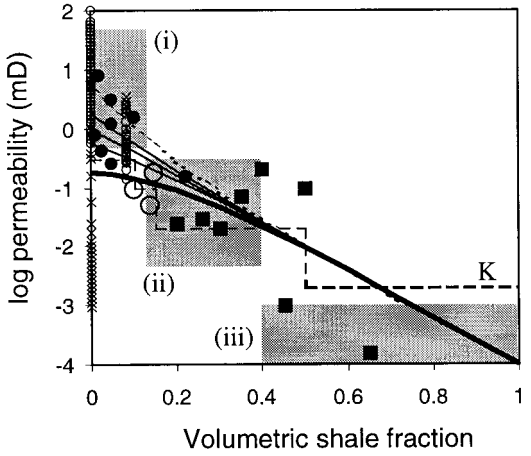

Fig. 2. Log permeability (mD) vs. volumetric shale fraction for fault-rock. Large data points are plug permeability measurements from core and outcrop samples from a variety of locations (Gibson 1998). Filled circles: cataclastic deformation bands. Open circles: solution deformation bands. Filled squares: clay gouge. Small data points are probe-permeability measurements of deformation bands (open circles) and slip surfaces (crosses) from sandstones in SE Utah (Antonellini & Aydin 1994). Boxes are summaries of data from the Sleipner Field (Ottesen Ellevset *et al.* 1998). (i) Cataclastic deformation bands. (ii) Framework phyllosilicate fault rocks. (iii) Shale smears. The line labelled 'K' represents average values, based on core samples from the Heidrun Field, used in a full-field flow simulation (Knai 1996). The curves (Equation 1) represent the relationship used in this work for permeability as a function of SGR (assumed equivalent to the fault-rock volumetric shale fraction) and displacement. Curves are given for D=1 mm (dashed line), D=10 cm, D=1 m, D=10 m and D=1 km (heavy line).

Fault zone thickness

Predicting fault zone thickness for sub-surface faults has been addressed recently by Childs *et al.* (1997) and Walsh *et al.* (1998*a*), so is not discussed in detail here. Fault zones comprise portions where two or more slip surfaces bound volumes of more or less deformed rock; and portions where the entire displacement is accommodated on single slip surfaces (lacunae). The thickness of the fault zone is defined as either the separation between the outermost slip surfaces (where more than one are present) minus the thickness of undeformed lenses, or the thickness of the slip-surface itself in a lacuna. Compilations of fault outcrop data (e.g. Robertson 1983; Hull 1988) demonstrate an approximately linear relationship between fault zone displacement and fault rock thickness (t_f) over several decades of scale-range with thickness values distributed over about two orders of magnitude for a particular displacement.

Figure 3 summarizes the data compiled by Hull (1988), and data from faults in mixed sandstone/shale sequences in Sinai (Knott *et al.* 1996), SE Utah (Foxford *et al.* 1998) and Lancashire, UK (Walsh *et al.* 1998*a*). Also plotted for several displacements are synthetic thickness values generated using the relationship:

$$t_f = D/66, \qquad (2)$$

to define a median thickness value, and a standard deviation for $\log t_f$ of 0.9 to define a log-normal thickness distribution. The data populate closely the envelopes defined by the outcrop studies for displacements over about 1 m. Equation 2 tends to under-predict the thickness of smaller faults but, as fault displacements less than 1 m are seldom incorporated in production flow simulation models, there is no need to predict accurately their thickness for this application.

Fault zone heterogeneity correlation-lengths

Fault zone properties are variable and unpredictable over short distances. Foxford *et al.* (1998) characterized the well-exposed Moab Fault in SE Utah over short sections at various locations

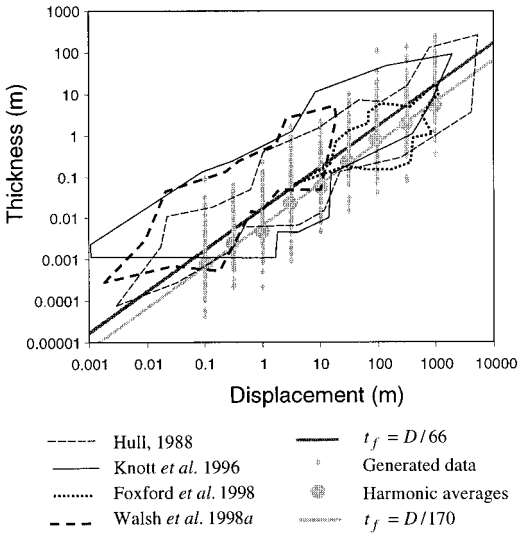

Fig. 3. Log thickness vs. log displacement (both in metres). Summaries of out-crop measurements are given as envelopes containing measurements from a variety of sources (Hull 1988), from faults in Nubian Sandstone in Western Sinai (Knott *et al.* 1996), from the Moab Fault in SE Utah (Foxford *et al.* 1998) and from faults in a Westphalian sandstone/shale sequence from Lancashire, UK (Walsh *et al.* 1998*a*). 200 log-normally-distributed thickness data (small diamonds) have been generated at various displacements with median value following the relationship $t_f = D/66$. The harmonic averages of these data (large circles) follow the relationship $t_f = D/170$.

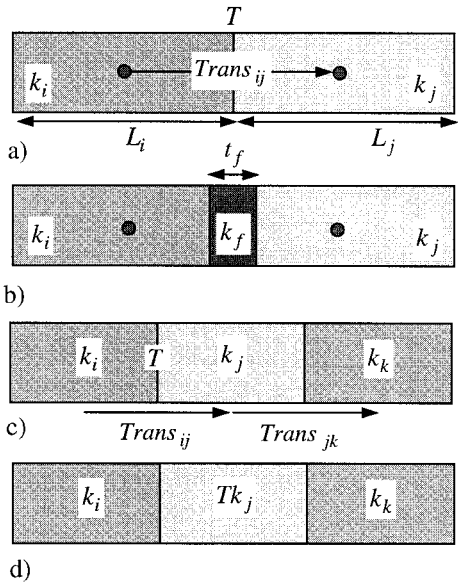

Fig. 4. Representation of a fault between grid-blocks *i* and *j*. (**a**) The transmissibility multiplier (*T*) acts on the transmissibility ($Trans_{ij}$) between two grid-block centres. $Trans_{ij}$ is a function of grid-block permeabilities and lengths. (**b**) To calculate the value of the multiplier, the thickness of low permeability fault-rock is considered explicitly. (**c**) A transmissibility multiplier assigned between blocks *i* and *j* modifies only $Trans_{ij}$. (**d**) A permeability multiplier applied to block *j* modified both $Trans_{ij}$ and $Trans_{jk}$.

along its 40 km trace and concluded that it is impossible to extrapolate predictions of the structure of the fault zone over distances greater than about 10 m. Similar fault zone thickness variability has been observed either in samples of different faults from the same sequence (e.g. Knott *et al.* 1996) or samples at different positions on the same fault trace (e.g. Blenkinsop 1989). The limited evidence available suggests that fault zone permeability is at least as heterogeneous as thickness (e.g. Fig. 2; Antonellini & Aydin 1994; Fowles & Burley 1994).

There are modelling advantages to fault zone structure being unpredictable over extremely small distances. The representative elementary volume (REV) of a correlated random field is about four times larger than the range of the semivariogram defining the field (Anguy *et al.* 1994). If the correlation length of fault zones is assumed to be in the order of 10–20 m, then the REV is in the order of 40–80 m. A typical reservoir simulation grid-block is about 100 m wide, and therefore contains a representative portion of a fault if the correlation length is as small as qualitative estimates suggest. As noted by Lopez & Smith (1996), correlation lengths of fault zones are extremely speculative, as the data necessary to address the issues fully do not exist. This is an area requiring further research, and for the purposes of this paper we assume a REV for fault zones exists, and that it is smaller than a reservoir grid-block. We make this assumption because it is convenient to do so: many aspects of fault zones, such as relay ramps, are likely to have correlation-lengths much larger than a grid-block. The implications of this discussion are addressed later in the paper.

In this section the relationships required for predicting the median permeability and thickness values of faults as a function of known details of the reservoir simulation model have been discussed. In the following section we discuss methods for incorporating the two orders of magnitude of variability of these values, at the sub-grid-block scale, into a single, up-scaled fault transmissibility value.

ANALYTICAL TRANSMISSIBILITY DETERMINATION

Fluxes in reservoir simulation models are calculated as a function of transmissibilities between pairs of grid-blocks. Transmissibilities are obtained by dividing the equivalent permeability of the blocks by the distance separating their centres (this assumes an intersection area of 1 and ignores grid-block dips – the precise details of calculating transmissibility differs between simulators – see, for example, Schlumberger GeoQuest 1995). For the pair of blocks illustrated in Fig. 4a, the transmissibility, $Trans_{ij}$, is

$$Trans_{ij} = \frac{2T}{\left(\frac{L_i}{k_i} + \frac{L_j}{k_j}\right)}, \tag{3}$$

where *T* is a transmissibility multiplier included to capture the effects of fault-rock between the two grid-blocks.

The properties of the fault-rock can be considered explicitly. If the fault has a thickness t_f and a permeability k_f (Fig. 4b), then the equivalent permeability between the centres of blocks *i* and *j* is:

$$k_e = \frac{L_i/2 + L_j/2}{\frac{L_i/2 - t_f/2}{k_i} + \frac{t_f}{k_f} + \frac{L_j/2 - t_f/2}{k_j}}, \tag{4}$$

and the transmissibility over this distance is:

$$Trans_{ij} = \frac{2}{\frac{L_i - t_f}{k_i} + \frac{2t_f}{k_f} + \frac{L_j - t_f}{k_j}}. \tag{5}$$

Equating 3 and 5 gives the transmissibility multiplier as a function of the dimensions and permeability of the grid-blocks and the thickness and permeability of the fault:

$$T=\left[1+t_{\mathrm{f}}\frac{(2/k_{\mathrm{f}}-1/k_i-1/k_j)}{(L_{\mathrm{i}}/k_{\mathrm{i}}+L_j/k_j)}\right]^{-1}. \quad (6)$$

For the special case where $L_i=L_j=L$ and $k_i=k_j=k_{\mathrm{m}}$, T becomes:

$$T=\left[1+\frac{t_{\mathrm{f}}}{L}\left(\frac{k_{\mathrm{m}}-k_{\mathrm{f}}}{k_{\mathrm{f}}}\right)\right]^{-1}, \quad (7)$$

which is equivalent to the transmissibility factor defined by Walsh *et al.* (1998*a*). For a case where $L_i\neq L_j$ or $k_i\neq k_j$, Equation 7 can be used as a multiplier on the permeability of one of the grid-blocks adjacent to the fault, effectively assigning the entire thickness of fault-rock to this cell. This provides the same transmissibility across the fault as applying Equation 6 to the interface between the two grid-blocks, but also modifies the transmissibility on the other side of the grid-block to which the permeability multiplier has been assigned. Therefore, the transmissibility multiplier (Equation 6, Fig. 4c) provides a numerically more robust representation of the fault than the permeability multiplier (Equation 7, Fig. 4d).

The dependencies implicit in a transmissibility multiplier are shown using a simplified Brent permeability sequence (after Walsh *et al.* 1998*b*). Two identical columns of grid-blocks are separated by an 80 m fault juxtaposing Tarbert and Ness against Rannoch, Etive and Broom (Fig. 5a). Implications of the practice of assigning a constant transmissibility multiplier to the entire fault are illustrated in Fig. 5b. Fault permeability has been back-calculated (using Equation 6) assuming a transmissibility multiplier of 0.3, a fault thickness of 1.2 m, and two model resolutions. This results in the geologically implausible situation in which the fault permeability depends on the permeabilities of the rock only immediately adjacent to the fault. Additionally, the back-calculated fault permeabilities have a meaningless dependence on the sizes of the grid-blocks (L).

Figure 5c illustrates the Shale Gouge Ratio method. Shale Gouge Ratio is calculated from the shale content of the faulted sequence, and provides a continuous log down the fault. SGR is converted to permeability, which is combined with the other variables in Equation 6 to calculate the fault transmissibility multipliers. The values of these multipliers are highly variable over short distances, but this variability reflects primarily the vertical heterogeneity of the original sequence: the fault permeability changes smoothly on the fault surface, reflecting the properties of the entire sequence which has moved past each particular grid-block.

Fault zone structure at a scale smaller than the vertical grid-block resolution is not captured by the SGR algorithm, and therefore SGR profiles which are based on the shale content of grid-blocks are more homogeneous than might be natural. We have discussed in the previous section that we expect at least two orders of magnitude variation in fault permeability at any particular SGR. This variability is intended to compensate for details in fault zone structure which are beyond the resolution of the model. Below, flow across a fault is considered analytically to determine the transmissibility of a representative portion of a heterogeneous fault. The implications of assumptions made in these determinations are investigated numerically using fine-scale flow simulation models in the following section.

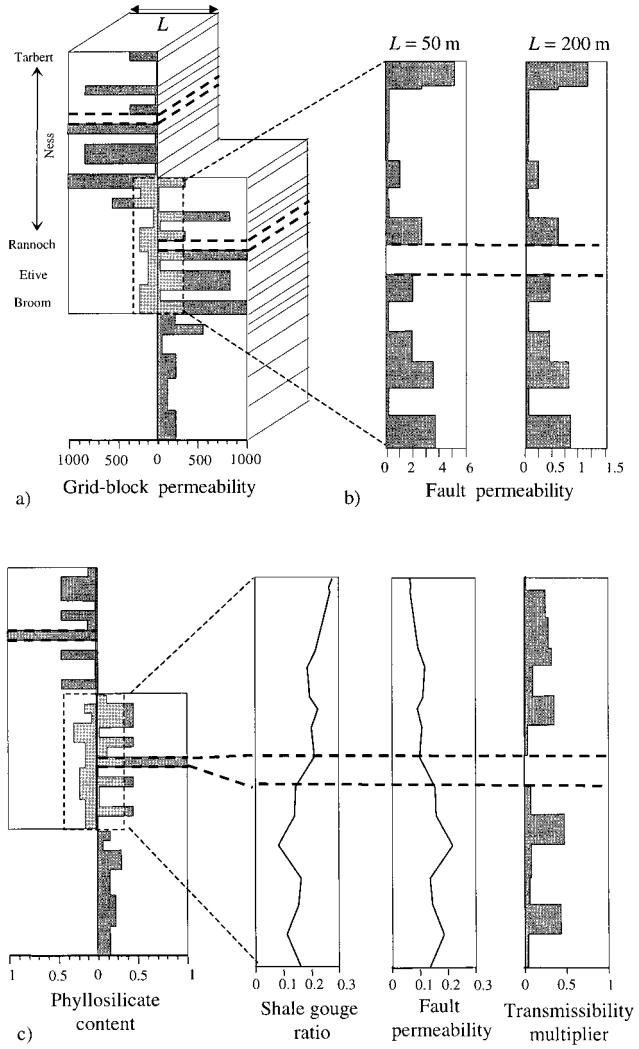

Fig. 5. Transmissibility multipliers for a simplified Brent sequence. The Mid-Ness shale is highlighted. (**a**) Sequence permeability (after Walsh *et al.* 1998*b*) is identical on both sides of the fault. (**b**) Fault permeability calculated as a function of a constant transmissibility multiplier $T=0.3$, fault thickness $t_{\mathrm{f}}=1.2$ m, and $L=50$ m and 200 m. (**c**) Fault transmissibility multiplier calculated using the SGR method for $t_{\mathrm{f}}=1.2$ m, and $L=100$ m.

Permeability and thickness averaging

The volumetric flow rate (q) across a homogeneous fault zone of cross-sectional area A, thickness t_{f} and permeability k_{f} is given by Darcy's Law:

$$q=\frac{k_{\mathrm{f}}}{\mu}A\frac{\Delta P}{t_{\mathrm{f}}}, \quad (8)$$

where ΔP is the pressure drop across the fault, and μ is the fluid viscosity. Assume that the fault is separated into elements A_1, $A_2 \ldots A_i \ldots A_n$, each of permeability k_{f1}, $k_{\mathrm{f2}} \ldots k_{\mathrm{f}i} \ldots k_{\mathrm{f}n}$ (Fig. 6a). Assume also that the pressure drop (ΔP) is identical across all elements. The volumetric flow rate in any element of the fault is:

$$q_i=\frac{k_{\mathrm{f}i}}{\mu}A_i\frac{\Delta P}{t_{\mathrm{f}}}, \quad (9)$$

and the total flow through the fault is given by:

$$q=\sum_{i=1}^{i=n}q_i=\frac{\Delta P}{\mu t_{\mathrm{f}}}\sum_{i=1}^{i=n}k_{\mathrm{f}i}A_i. \quad (10)$$

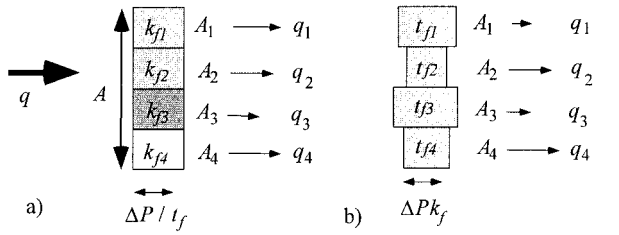

Fig. 6. Calculation of the equivalent permeability of heterogeneous faults. (**a**) Variable permeability, constant thickness. (**b**) Variable thickness, constant permeability. In each case the pressure drop across the fault is considered constant. See text for discussion.

Equating 8 and 10 gives:

$$k_{\mathrm{f}} = \frac{1}{A} \sum_{i=1}^{i=n} k_{\mathrm{f}i} A_i, \tag{11}$$

which is, by definition, the area-weighted arithmetic average permeability.

Consider a similar situation to the one discussed above, with the difference that each fault element A_i now has a constant permeability k_{f} but a variable thickness $t_{\mathrm{f}i}$. Again, the total pressure drop across each fault element is considered constant (Fig. 6b). In this case the total volumetric flow is given by:

$$q = \sum_{i=1}^{i=n} q_i = \frac{\Delta P k_{\mathrm{f}}}{\mu} \sum_{i=1}^{i=n} \frac{A_i}{t_{\mathrm{f}i}}. \tag{12}$$

Equating 8 and 12 gives:

$$t_{\mathrm{f}} = A \left[\sum_{i=1}^{i=n} \frac{A_i}{t_{\mathrm{f}i}} \right]^{-1}, \tag{13}$$

which is the area-weighted harmonic average thickness.

Equations 11 and 13 give the permeability and thickness input required to up-scale the transmissibility of heterogeneous faults.

Transmissibility determination from geological input

We have defined the variables which influence fault transmissibility, methods for estimating the median values of these variables as a function of the reservoir model, and have defined analytically the appropriate averages for representing the heterogeneity in these variables. Below we calculate these thickness and permeability averages as a function of their median values.

We assume that both thickness and permeability vary over the area of a grid-block according to a log-normal distribution. The median value of a log-normal distribution is the mean of the normal distribution of the log-variable. For a log-normal distribution with a log-variable mean, μ, and standard deviation, σ, the arithmetic average of the distribution is $10^{(\mu+\sigma^2/2)}$, and the harmonic average is $10^{(\mu-\sigma^2/2)}$. For any particular SGR and displacement, we assume that the median permeability and thickness values are given by Equations 1 and 2, in each case with $\sigma = 0.9$. This standard deviation is equivalent to about 75% of the values lying within $\pm$ one order of magnitude of the median, and 90% lying within ± 1.5 orders of magnitude (Fig. 3). For thickness, $\mu = \log(D/66)$, $\sigma = 0.9$ gives the harmonic average thickness as a function of displacement:

$$t_{\mathrm{f}b} = \mathrm{D}/170. \tag{14}$$

For permeability,

$$\mu = -4\mathrm{SGR} - \frac{1}{4}\log(D)(1-\mathrm{SGR})^5$$

and $\sigma = 0.9$ gives the arithmetic average permeability as a function of SGR and displacement:

$$\log k_{\mathrm{f}a} = 0.4 - 4\mathrm{SGR} - \frac{1}{4}\log(D)(1-\mathrm{SGR})^5. \tag{15}$$

Incorporating Equations 14 and 15 into Equation 6 gives the appropriately up-scaled transmissibility multiplier for each grid-block fault-face, and into Equation 7 gives a permeability multiplier for each grid-block on one side of the fault.

Application to a full-field simulation model

The method has been applied to calculate fault multipliers to a full-field (Eclipse) flow simulation model of a North Sea Brent reservoir. The 24 000 grid-block model contains 96 000 vertical grid-block faces, of which over 14 000 are faulted. Code has been written which reads in the Eclipse format corner-point geometry and directional grid-block permeability files, along with another file listing the phyllosilicate (or *V*shale) content of each grid-block. The latter file is the only input which is not also an input into the flow simulator. Phyllosilicate content was used while building the stochastic sedimentological reservoir model, and therefore generation of this file does not add to the overall workflow. These files between them contain all the information necessary to calculate individual transmissibility multipliers for each fault-face, via intermediary calculations of fault displacement and SGR, and the output of the program can be input directly into the simulator. Figure 7 shows fault surface maps for one fault in the model, with the output as either permeability multipliers (Equation 7) or transmissibility multipliers (Equation 6).

The thickness of the fault is calculated as a function of the displacement at each cell centre (Fig. 7b). Flow between each pair of connected grid-blocks is a function of the permeability of these grid-blocks (Fig. 7c,d) and the area of each grid-block to grid-block intersection. Figure 7e shows the transmissibility (normalized by intersection area) for the fault surface, based on grid-block connections and assuming no fault properties. The fault properties are calculated as a function of the shale content of the grid-block (Fig. 7f and g) to provide an SGR map (Fig. 7h) which is combined with fault displacement to obtain a fault permeability map (Fig. 7i). Fault permeability multipliers acting on the hangingwall grid-block permeabilities (Fig. 7c) are shown on Fig. 7j, and fault transmissibility multipliers acting on block to block transmissibilities are shown on Fig. 7k. The transmissibility multiplier requires greater definition than the permeability multiplier, as a value must be calculated for each connection.

Heterogeneity in the value of either multiplier reflects both the smooth variation in fault zone properties and the rapid variation in grid-block permeabilities. The first influence provides the overall trends in the multiplier. For instance, in the area of the fault surface between the hangingwall and footwall cut-offs of the Mid-Ness shale, SGR is high, fault permeability is low and the multipliers are generally low. More rapid variation in grid-block permeabilities locally overprints the relatively smooth variation caused by the fault zone properties, for instance in the area with high transmissibility multipliers two grid-blocks above the hangingwall cut-off of the Mid-Ness shale. Fault permeability is low in this area, but the value of the

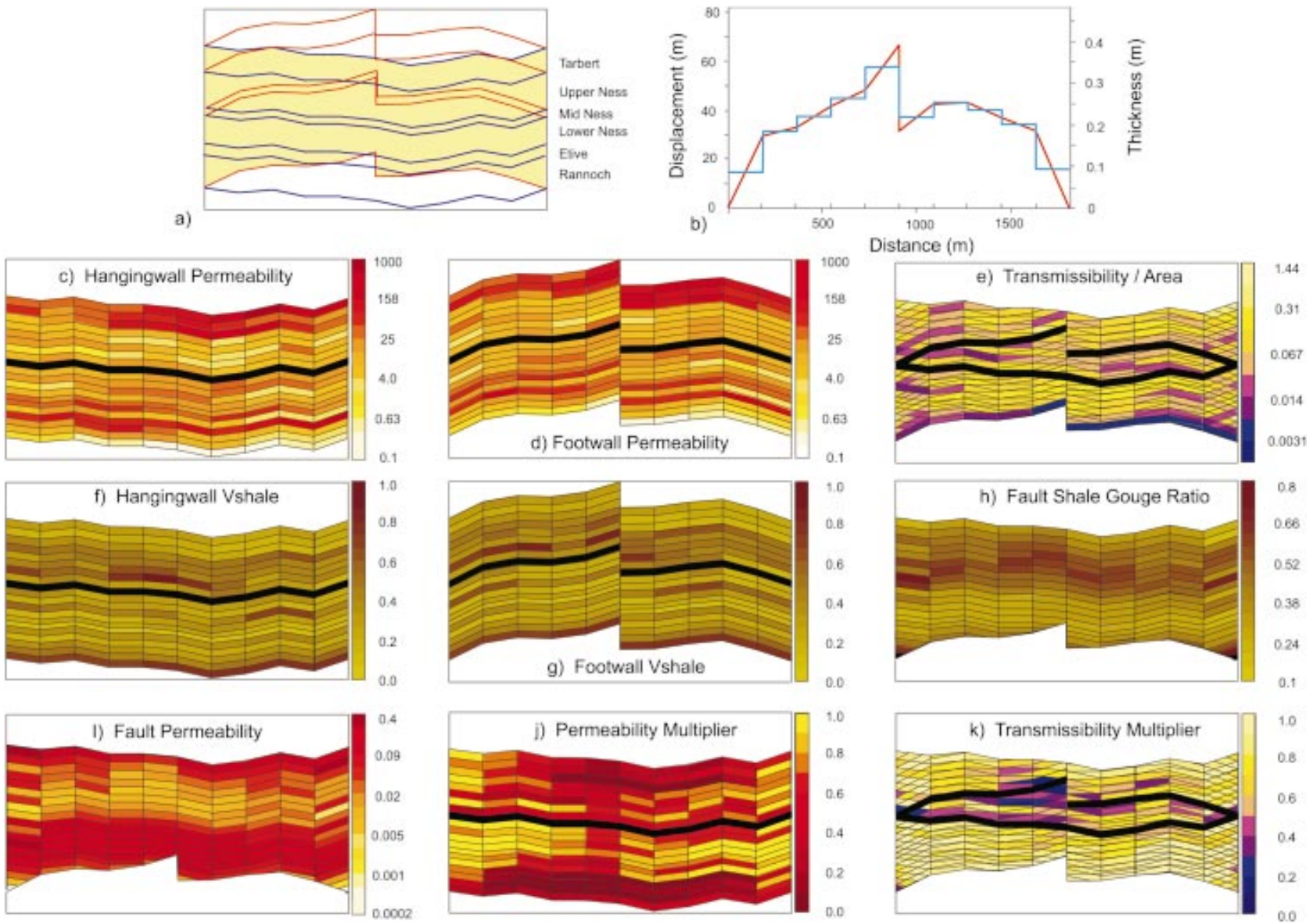

Fig. 7. Fault transmissibility and permeability multipliers for a fault in a Brent sequence reservoir simulation model. The 20 layer model is 195 m thick, and the fault is 1833 m long (10 cells). The fault has an out-of-plane footwall splay. The inactive Mid-Ness shale is black. (**a**) Summary of the fault surface. All hangingwall cut-offs (blue) and some footwall cut-offs (red) are shown. The yellow area represents the region over which the active grid-cells are juxtaposed. (**b**) Fault thickness (blue) is calculated at grid-block centres from the fault displacement (red). (**c**) Hangingwall permeability (mD, log scale). (**d**) Footwall permeability (mD, log scale). (**e**) Transmissibility/area, assuming no fault properties (mD m^{-1}, log scale). (**f**) Hangingwall phyllosilicate content (fraction). (**g**) Footwall phyllosilicate content (fraction). (**h**) Fault surface SGR calculated for the hangingwall grid-blocks (fraction). (**i**) Fault permeability calculated for the hangingwall grid-blocks (mD, log scale). (**j**) Fault permeability multiplier calculated for the hangingwall grid-blocks (linear scale). (**k**) Fault transmissibility multiplier (linear scale). See text for discussion.

multiplier is responding to a locally low permeability in the hangingwall section of Upper Ness.

The method provides fault multiplier models of much higher resolution than is usual. This high resolution is necessary as the permeability of the grid-blocks is more heterogeneous than the predicted fault properties, and both determine the values of the multiplier. The method is based on a geological model of the faults, and the factors which most influence fault zone content are fault displacement and details of the faulted sedimentary succession, both of which change rapidly at the resolution of a simulation model. As fault zone content depends on the sedimentology, any stochastic realization of the reservoir sedimentology requires a new generation of the fault permeabilities, but more importantly requires a new set of multipliers, as these depend additionally on the grid-block permeabilities.

Fault zone permeability and thickness prediction is imprecise and there is potential for changing the predictors (Equations 14 and 15) systematically to match the particular behaviour observed during the production history of a field (e.g. Fulljames *et al.* 1997). The advantage of the proposed method is that it is based on a geological model of fault zone content, and therefore any change in fault transmissibility values needed, effects an improvement in the understanding of the fault characteristics in the reservoir. In the following section we investigate some of the assumptions involved in up-scaling fault transmissibility, using fine-scale numerical flow simulations.

NUMERICAL VALIDATION

Several assumptions were made in the analytical up-scaling solution for fault transmissibility, and we use numerical flow simulation to illustrate the significance of two of them. The first assumption is that fault zone permeability and thickness can be considered independently. Fault growth models (e.g. Childs *et al.* 1996) and field data (e.g. Knott *et al.* 1996) suggest that fault zone thickness varies as a function of the faulted lithologies, which is also the primary control on permeability. Therefore spatial variations in fault zone permeability and thickness are not necessarily independent. The second assumption made is that there is a constant pressure drop across each fault element. A third assumption, that the REV of a fault zone is smaller than a full-field simulator grid-block, is also discussed.

Figure 8 shows a cartoon of the flow simulation scheme used. The models are 3D with matrix permeability constant in any model (but variable between models), and a heterogeneous fault zone crossing the centre of the model. As matrix permeability is constant, Equation 7 is appropriate for calculating the transmissibility multiplier. The fault comprises 2500 elements (each 10 cells wide) assigned uniformly, log-uniformly, normally or log-normally distributed permeability and thickness values arranged randomly. As the spatial distributions of fault zone properties is random, the REV of the fault zone is much smaller than the model cross-sectional area. Fault thickness in the simulation model is held constant as a modelling simplification, but the influence of thickness is one we wish to examine. By manipulating Equation 7, we calculate a new permeability for each fault element, which incorporates the influence of both the permeability and thickness assigned to it. Therefore the model fault contains the desired variability in both permeability and thickness. Constant flow rate boundary conditions are imposed between the two faces parallel to the fault, and periodic boundary conditions are applied on the other four faces. The equivalent permeability of the entire model parallel to the flow direction is calculated from the observed

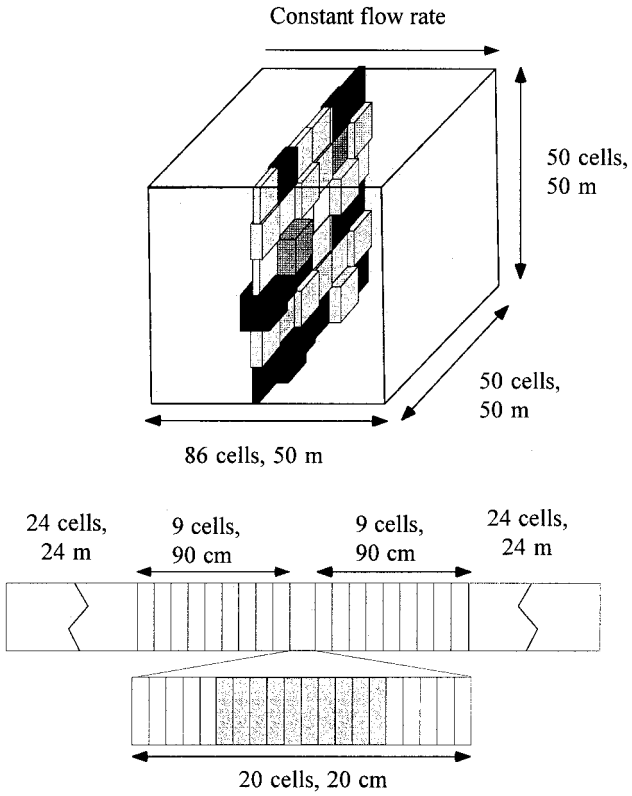

Fig. 8. Cartoon of the flow simulation scheme, highlighting the discretization used in the flow direction. The matrix is homogeneous, and the fault is composed of 2500 fault elements with randomly arranged permeability and thickness values.

pressure drop, and the equivalent fault permeability is determined using the harmonic average. This value is used to calculate an equivalent transmissibility multiplier for the entire 50 × 50 × 25 m region of the model up-stream of the fault.

Spatial correlation of permeability and thickness

Figure 9a compares transmissibility derived analytically using the appropriate thickness and permeability averages in Equation 7 with transmissibility determined from numerical simulation. Transmissibility is predicted well by the analytical solution only if there is no spatial correlation between fault permeability and thickness. If derived analytically, transmissibility is over-estimated if there is a positive correlation between thickness and permeability, and under-estimated for a negative correlation. This error arises because a positive correlation will tend to reduce the variability of q_i, as the flow rate across a thin element of low permeability might be similar to the flow rate through a thicker, more permeable element. Therefore, use of the arithmetic and harmonic averages tends to overcompensate for the variability. Conversely, when thickness and permeability are inversely correlated, the variability in flow rate is much greater than is predicted by the simple averages. Equation 9 shows that through a homogeneous element of a fault containing variability in both thickness and permeability,

$$q_i \propto \frac{k_{\mathrm{f}i} A_i}{t_{\mathrm{f}i}}. \tag{16}$$

Therefore, if the permeability/thickness ratio is calculated in each region of the fault, and the area-weighted arithmetic average of this ratio is taken, then this average incorporates the

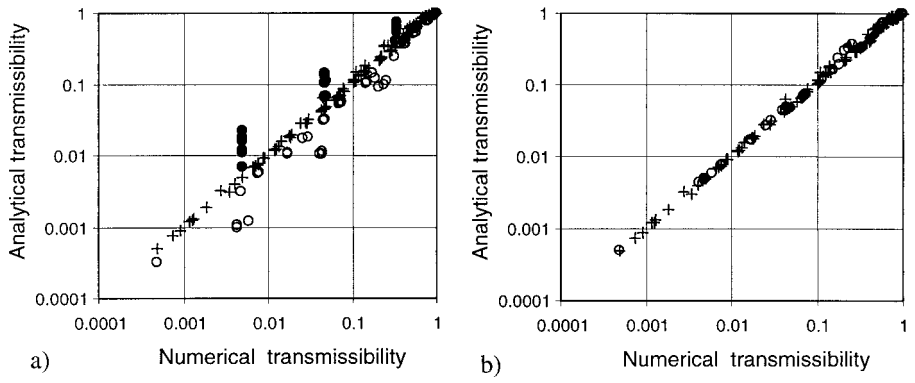

Fig. 9. Flow simulation results for a variety of heterogeneous faults in a homogeneous matrix. (**a**) Analytical transmissibility calculated with Equation 7, vs. transmissibility determined from numerical simulation results. Crosses: no thickness/permeability correlation; filled circles: positive correlation; open circles: negative correlation. (**b**) As (a), except the analytical transmissibility has been calculated using Equation 17.

effects of both variables irrespective of the correlation between them. Hence the equivalent transmissibility should be determined as a function of the arithmetic average of the fault permeability/thickness ratio $(k_f/t_f)_a$. Equations 6 and 7, however, have no solution as a function of this ratio. The approximation to Equation 7:

$$T=\left[1+\left(\frac{k_m-k_{fa}}{L(k_f/t_f)_a}\right)\right]^{-1} \tag{17}$$

may be made, but this includes the k_{fa} term independently of the t_f term. Equation 16 indicates that to calculate correctly the flow response through a fault in which thickness and permeability variations are correlated, these variables should not be separated. Nevertheless, Fig. 9b shows that Equation 17 provides a considerably more accurate estimate of transmissibility than is achieved by considering each variable separately.

Flow segregation through a heterogeneous fault

The second assumption in the analytical transmissibility solution is that the pressure drop across each fault element is constant (Fig. 6), and that the flow through each fault element is given by Equation 9. The suitability of the assumption is examined by comparing the distribution in flow through each element predicted analytically, with that obtained numerically.

Based on Equation 9, which relies on the constant pressure drop assumption, the fraction of the total flow through the fault which passes through any fault element is:

$$\frac{q_i}{q}=\frac{k_{fi}}{t_{fi}}\Big/\sum_{i=1}^{i=n}\frac{k_{fi}}{t_{fi}} \tag{18}$$

We consider a fault with permeability and thickness values each distributed over two orders of magnitude. Figure 10 shows a plot of cumulative flow fraction (q_i/q) vs. cumulative fault area for this fault. This plot is similar to the Lorenz curve and reflects flow heterogeneity (e.g. Lake & Jensen 1991). The curve indicates that extreme flow segregation must occur within the fault if the equivalent fault transmissibility matches that predicted analytically. For this fault, the least transmissible 30% of the fault surface area contributes less than 1% of the total flow, 90% of the total flow occurs through the most transmissible 30% of the fault and 50% of the flow occurs through less than 6% of the fault. If the flow segregation observed in flow models closely approximates that predicted using Equation 18, then the assumption of a constant pressure drop across the fault is acceptable.

On Fig. 11 the flow segregation obtained through heterogeneous faults in two numerical flow simulations is compared with the curves calculated according to Equation 18. A fault with log-normally distributed values of k_f and an arithmetic average permeability of 0.0512 mD is placed in a 10 mD and 10 D matrix. Figure 11a shows that in the low matrix permeability (high fault transmissibility) case, there is more flow through most of the fault surface than is predicted analytically. The difference becomes significant however, when the numerical/analytical flow is plotted as a function of the cumulative flow through the fault (Fig. 11b). This representation shows that the 95% of fault surface through which there is more flow than predicted accounts for only 60% of the total flow. In the 5% of fault surface which controls 40% of the total flow there is less flow than predicted.

There is less flow segregation through this fault than the analytical result predicts, and this reduces the equivalent fault permeability. The numerical equivalent fault permeabilities are 0.0355 mD in the low matrix permeability case and 0.0505 mD in the high matrix permeability case. For the high matrix permeability case (curve (ii) on Fig. 11) the modest reduction in permeability with respect to the analytical estimation is caused by the slight dip in the curve at the highest flux element, but on the whole the numerical curve matches well with the analytical one, and the equivalent permeability is close to the analytical estimate.

The fault is identical in both models, only the matrix permeability in which the fault is contained is different, so the differences in the equivalent fault permeability are a function of the matrix permeability. In order to satisfy the assumption of a constant pressure drop across the fault, there must be sufficient transmissibility up-stream and down-stream of the fault for the flow paths to become optimally arranged to accommodate the flow segregation which must occur. If the model dimensions or the matrix permeability are increased, the equivalent fault permeability is larger, as more tortuous flow is possible outside

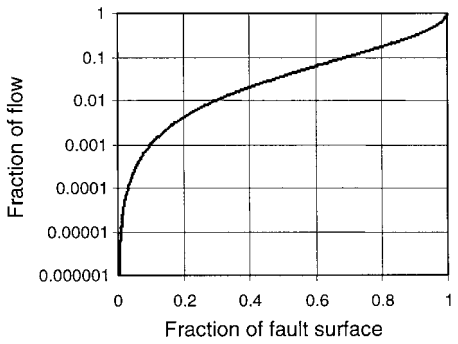

Fig. 10. Fraction of flow through a fault vs. fraction of fault surface. Data are sorted in terms of increasing flow fraction. See text for discussion.

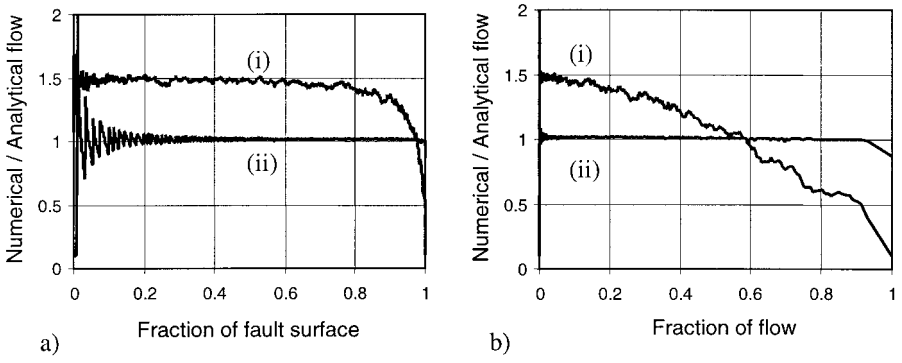

Fig. 11. Comparisons of numerical with analytical flow as a function of (**a**) the fault surface area, and (**b**) the analytical flow distribution (see Fig. 10). The arithmetic average fault permeability is 0.0512 mD. Curve (i): low matrix permeability; equivalent fault permeability is 0.0355 mD. Curve (ii): high matrix permeability; equivalent fault permeability is 0.0505 mD.

the fault to accommodate an ideally heterogeneous distribution of flow through the fault. If the permeability of the fault is high compared to the permeability of the matrix, then the fault heterogeneity is influential on flow paths for greater distances outside the fault.

These examples have shown that the assumption of a constant pressure drop across a heterogeneous fault is incorrect, and that analytically derived transmissibility will systematically over-estimate the fault transmissibility at high transmissibility and/or for a highly heterogeneous k_f/t_f fault structure. However, the errors are not large (Fig. 9b), and the values calculated according to the arithmetic average of the permeability/thickness ratio provide a reasonable approximation of fault transmissibility multipliers calculated using numerical simulation models.

Fault zone representivity and boundary conditions

In the examples discussed above, the equivalent fault permeability of identical faults is shown to vary as a function of the permeability of the matrix in which the fault is contained. This is a different effect to the one discussed by Walsh *et al.* (1998*a*), who showed that the transmissibility of statistically identical faults decreases as the correlation-lengths of the fault increases. In their models, the matrix permeability and model dimension are constant, and the differences in permeability are a function of sampling an area which is smaller than the fault's REV. If a larger portion of the fault had been modelled, then the equivalent fault permeability would have been higher. If a fault's REV is larger than a simulator grid-block, then the transmissibility of a particular fault-face will be different to the transmissibility of a representative portion of the fault. As discussed for an analogous situation by Begg *et al.* (1989), the overall transmissibility of the fault is adequately represented by assigning the REV-scale equivalent property to each fault-face, although this results in a more homogeneous fault model than is actually present at the resolution of the simulation model.

In the models described in this paper, the area considered is larger than the REV, and the differences in equivalent fault permeability are caused by different model boundary conditions in the flow direction, rather than by the no-flow boundary conditions on the other four faces, as they are in the models described by Walsh *et al.* (1998*a*). The control of boundary conditions of the kind influencing the modelling described here are relevant in the sub-surface, as they are controlled by the overall permeability structure of the reservoir.

SUMMARY

This paper has presented and discussed a geologically driven method for calculating fault transmissibility multipliers for reservoir flow simulation models as a function of known details of the simulation model. Transmissibility multipliers for grid-block fault-faces vary as a function of the dimensions and permeabilities of the grid-blocks to which they are attached, and of the fault permeability and thickness. Fault permeability and thickness values vary by at least two orders of magnitude over short distances, and their median values can be estimated using empirical relationships linking fault permeability to fault displacement and Shale Gouge Ratio (SGR), and fault thickness to displacement. Analytical considerations show that these empirical relationships must be modified to incorporate the influence of sub-grid-block scales of property variability, and these modifications are supported by numerical flow simulation. The method allows fault properties for every grid-block fault-face to be calculated as a function of:

- the phyllosilicate content of the grid-blocks,
- the grid-block permeabilities and
- the grid geometry.

Fault properties are incorporated in the simulation model either as directional permeability multipliers assigned to the grid-blocks on one side of the fault or, more rigorously, as transmissibility multipliers defined explicitly for each grid-block to grid-block connection. The method has been applied to a full-field reservoir simulation model.

CONCLUSIONS

We have incorporated geological conceptualizations of fault zone structure and content into a predictive method for calculating fault zone transmissibility multipliers. This method is based on poorly defined empirical correlations which can only be improved when more data become available.

Numerical and analytical considerations of flow through realistically heterogeneous faults have highlighted the following:

- Flow through a representative portion of a heterogeneous fault can be approximated as a function of the harmonic average of the fault zone thickness and the arithmetic average of the fault zone permeability, provided there is no spatial correlation of permeability and thickness.
- Where there is spatial correlation of permeability and thickness, the transmissibility of the fault is a function of the arithmetic average of the permeability/thickness ratio. There is, however, no analytical solution to transmissibility as a function of this ratio.
- Extreme flow segregation occurs through realistically heterogeneous faults. This flow segregation is accommodated by tortuous flow in the matrix.
- The analytical determination systematically overestimates fault transmissibility at higher fault transmissibilities and

higher fault heterogeneities. The extent of this over-estimation is a function of the permeability structure to significant distances down-stream and up-stream of the fault, as this determines the ease of tortuous flow in the matrix.

- Statistically identical faults do not necessarily have the same transmissibility even if an area larger than the REV is being modelled. In a system containing statistically identical heterogeneous faults, the more closely spaced faults will have a lower transmissibility.

This work was carried out during projects funded by the DTI Hydrocarbon Reservoir Link Programme (Project 7246), the DTI/OGPSO Programme (Project 7234) and the EU Hydrocarbon Reservoir Research Programme (Contract JOF3-CT95-0006). The simulation model was built in conjunction with G. Aadmodt, O. Lia and H. Omre from the Norwegian Computing Centre and K. Geel from TU Delft. We thank these colleagues, two anonymous reviewers, and members of the Fault Analysis Group, particularly J. Watterson and C. Childs, for useful discussion.

REFERENCES

ALLAN, U. S. 1989. Model for hydrocarbon migration and entrapment within faulted structures. *American Association of Petroleum Geologists Bulletin*, **73**, 803–811.

ANGUY, Y., EHRLICH, R., PRINCE, C. M., RIGGERT, V. L. & BERNARD, D. 1994. The sample support problem for permeability assessment in sandstone reservoirs. *In*: Yarus, J. M. & Chambers, R. L. (eds) *Stochastic modeling and geostatistics*. American Association of Petroleum Geologists, Computer Applications in Geology Series, **3**, 37–54.

ANTONELLINI, A. & AYDIN, A. 1994. Effect of faulting on fluid flow in porous sandstones: petrophysical properties. *American Association of Petroleum Geologists Bulletin*, **78**, 181–201.

——, —— & POLLARD, D. D. 1994. Microstructure of deformation bands in porous sandstones at Arches National Park, Utah. *Journal of Structural Geology*, **16**, 941–959.

BEGG, S. H., CARTER, R. R. & DRANFIELD, P. 1989. Assigning effective values to simulator gridblock prarameters for heterogeneous reservoirs. *SPE Reservoir Engineering*, **November 1989**, 455–463.

BENTLEY, M. R. & BARRY, J. J. 1991. Representation of fault sealing in a reservoir simulation: Cormorant block IV UK North Sea. *In*: *66th Annual Technical Conference & Exhibition of the Society of Petroleum Engineers*, Dallas Texas, 119–126.

BLENKINSOP, T. G. 1989. Thickness–displacement relationships for deformation zones: Discussion. *Journal of Structural Geology*, **11**, 1051–1054.

BOUVIER, J. D., KAARS-SIJPESTEIJN, C. H., KLUESNER, D. F., ONYEJEKWE, C. C. & VAN DER PAL, R. C. 1989. Three-dimensional seismic interpretation and fault sealing investigations, Nun River Field, Nigeria. *American Association of Petroleum Geologists Bulletin*, **73**, 1397–1414.

CHILDS, C., WALSH, J. J. & WATTERSON, J. 1997. Complexity in fault zones and implications for fault seal prediction. *In*: Møller-Pedersen, P. & Koestler, A. G. (eds) *Hydrocarbon Seals: Importance for Exploration and Production*. Special publication of the Norwegian Petroleum Society, **7**, 61–72.

——, WATTERSON, J. & WALSH, J. J. 1996. A model for the structure and development of fault zones. *Journal of the Geological Society, London*, **153**, 337–340.

CRAWFORD, B. R. 1998. Experimental fault sealing: shear band permeability dependency on cataclastic fault gouge characteristics. *In*: Coward, M. P., Johnson, H. & Daltaban, T. (eds) *Structural Geology in Reservoir Characterisation*. Geological Society, London, Special Publications, **127**, 27–44.

EVANS, J. P., FORSTER, C. B. & GODDARD, J. V. 1997. Permeability for fault related rocks and implication for hydraulic structure of fault zones. *Journal of Structural Geology*, **19**, 1393–1404.

FOWLES, J. & BURLEY, S. 1994. Textural and permeability characteristics of faulted, high porosity sandstones. *Marine and Petroleum Geology*, **11**, 608–623.

FOXFORD, K. A., WALSH, J. J., WATTERSON, J., GARDEN, I. R., GUSCOTT, S. C. & BURLEY, S. D. 1998. Structure and content of the Moab Fault Zone, Utah, USA and its implication for fault seal predictions. *In*: Jones, G., Fisher, Q. J. & Knipe, R. J. (eds) *Faulting, Fault Sealing and Fluid Flow in Hydrocarbon Reservoirs*. Geological Society, London, Special Publications, **147**, 87–103.

FRISTAD, T., GROTH, A., YIELDING, G. & FREEMAN, B. 1997. Quantitative fault seal prediction – A case study from Oseberg Syd. *In*: Møller-Pedersen, P. & Koestler, A. G. (eds) *Hydrocarbon Seals: importance for exploration and production*. Special Publication of the Norwegian Petroleum Society, **7**, 107–124.

FULLJAMES, J. R., ZIJERVELD, J. J. & FRANSSEN, C. M. W. 1997. Fault seal processes: systematic analysis of fault seals over geological and production time scales. *In*: Møller-Pedersen, P. & Koestler, A. G. (eds) *Hydrocarbon Seals: importance for exploration and production*. Special Publication of the Norwegian Petroleum Society, **7,** 51–59.

GIBSON, R. G. 1994. Fault-Zone seals in siliciclastic strata of the Columbus Basin, offshore Trinidad. *American Association of Petroleum Geologists Bulletin*, **78**, 1372–1385.

—— 1998. Physical character and fluid-flow properties of sandstone derived fault gouge. *In*: Coward, M. P., Johnson, H. & Daltaban, T. (eds) *Structural Geology in Reservoir Characterization*. Geological Society, London, Special Publications, **127**, 83–97.

HULL, J. 1988. Thickness–displacement relationships for deformation zones. *Journal of Structural Geology*, **10**, 431–435.

KNAI, T. A. 1996. Faults impact on fluid flow in the Heidrun Field. In: *Faulting, Fault Sealing and Fluid Flow in Hydrocarbon Reservoirs*, University of Leeds, Leeds, 75. (Abstract)

KNIPE, R. J. 1997. Juxtaposition and seal diagrams to help analyze fault seals in hydrocarbon reservoirs. *American Association of Petroleum Geologists Bulletin*, **81**, 187–195.

KNOTT, S. D., BEACH, A., BROCKBAND, P. J., BROWN, J. L., McCALLUM, J. E. & WELDON, A. I. 1996. Spatial and mechanical controls on normal fault populations. *Journal of Structural Geology*, **18**, 359–372.

LAKE, L. W. & JENSEN, J. L. 1991. A review of heterogeneity measures used in reservoir characterisation. *In situ*, **15**, 409–437.

LIA, O., OMRE, H., TJELMELAND, H., HOLDEN, L. & EGELAND, T. 1997. Uncertainties in reservoir production forecasts. *American Association of Petroleum Geologists Bulletin*, **81**, 775–801.

LINDSAY, N. G., MURPHY, F. C., WALSH, J. J. & WATTERSON, J. 1993. Outcrop studies of shale smears on fault surfaces. *In*: Flint, S. & Bryant, A. D. (eds) *The Geological Modelling of Hydrocarbon Reservoirs and Outcrop*. International Association of Sedimentology, **15**, 113–123.

LOPEZ, D. L. & SMITH, L. 1996. Fluid flow in fault zones: influence of hydraulic anisotropy and heterogeneity on the fluid flow and heat transfer regime. *Water Resources Research*, **32**, 3227–3235.

MANZOCCHI, T., RINGROSE, P. S. & UNDERHILL, J. R. 1998. Flow through fault systems in high porosity sandstones. *In*: Coward, M. P., Johnson, H. & Daltaban, T. (eds) *Structural Geology in Reservoir Characterization*. Geological Society, London, Special Publications, **127**, 65–82.

OTTESEN ELLEVSET, S., KNIPE, R. J., OLSEN, T. S., FISHER, Q. T. & JONES, G. 1998. Fault controlled communication in the Sleipner Vest Field, Norwegian Continental Shelf: detailed, quantitative input for reservoir simulation and well planning. *In*: Jones, G., Fisher, Q. J. & Knipe, R. J. (eds) *Faulting, Fault Sealing and Fluid Flow in Hydrocarbon Reservoirs*. Geological Society, London, Special Publications, **147**, 283–297.

ROBERTSON, E. C. 1983. Relationship of fault displacement to gouge and breccia thicknesses. *Institute of Mining Engineers*, **35**, 1426–1432.

SCHLUMBERGER GEOQUEST 1995. *Eclipse 100 technical description*, 96A.

WALSH, J. J., WATTERSON, J., HEATH, A. E. & CHILDS, C. 1998*a*. Representation and scaling of faults in fluid flow models. *Petroleum Geoscience*, **4**, 241–251.

——, ——, ——, GILLESPIE, P. A. & CHILDS, C. 1998*b*. Assement on the effects of sub-seismic faults on bulk permeabilities of reservoir sequences. *In*: Coward, M. P., Johnson, H. & Daltaban, T. (eds) *Structural Geology in Reservoir Characterisation*. Geological Society, London, Special Publications, **127**, 99–114.

WATTS, N. L. 1987. Theoretical aspects of cap-rock and fault seals for single- and two-phase hydrocarbon columns. *Marine and Petroleum Geology*, **4**, 274–307.

YIELDING, G., FREEMAN, B. & NEEDHAM, D. T. 1997. Quantitative fault seal prediction. *American Association of Petroleum Geologists Bulletin*, **81**, 897–917.

Received 3 March 1998, revised typescript accepted 21 September 1998.